A novel method for autonomous remote condition monitoring of rotating machines using piezoelectric energy harvesting approach

Khazaee, Majid; Rezaniakolaei, Alireza; Moosavian, Ashkan; Rosendahl, Lasse

Published in:
Sensors and Actuators A: Physical

DOI (link to publication from Publisher):
10.1016/j.sna.2019.05.016

Publication date:
2019

Document Version
Accepted author manuscript, peer reviewed version

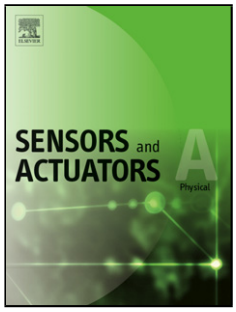

Title: A novel method for autonomous remote condition monitoring of rotating machines using piezoelectric energy harvesting approach

Authors: Majid Khazaee, Alireza Rezaniakolaie, Ashkan Moosavian, Lasse Rosendahl

PII: S0924-4247(19)30414-5
DOI: https://doi.org/10.1016/j.sna.2019.05.016
Reference: SNA 11388

To appear in: *Sensors and Actuators A*

Received date: 14 March 2019
Revised date: 8 May 2019
Accepted date: 11 May 2019

Please cite this article as: Khazaee M, Rezaniakolaie A, Moosavian A, Rosendahl L, A novel method for autonomous remote condition monitoring of rotating machines using piezoelectric energy harvesting approach, *Sensors and amp; Actuators: A. Physical* (2019), https://doi.org/10.1016/j.sna.2019.05.016

A novel method for autonomous remote condition monitoring of rotating machines using piezoelectric energy harvesting approach

Majid Khazaee[1], Alireza Rezaniakolaie[*1], Ashkan Moosavian[2] , Lasse Rosendahl[1]

[1] *Department of Energy Technology, Aalborg university, Pontopisanstraede 111, DK 9220, Aalborg, Denmark.*

[2] *Department of Mechanical Engineering of Agricultural Machinery, Tarbiat Modares University, Jalal AleAhmad, Nasr, Tehran, Iran.*

[*] Corresponding Author; *E-mail address:* alr@et.aau.dk.

Graphical abstract

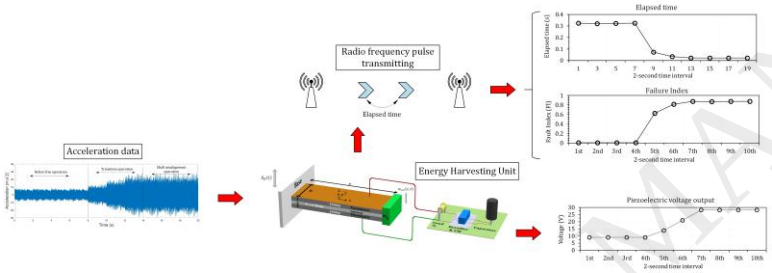

Highlights

- Centrifugal rotating machines are suitable for piezoelectric energy harvesting.
- Piezoelectric provides adequate energy for microprocessor and wireless transmitter.
- 5-stage Dickson Charge Pump increased piezoelectric voltage 74%.
- Piezoelectric power during operation varies considerably with machine condition.
- Autonomous condition monitoring is performed using pulse elapse time tracking.

Abstract

This paper presents a novel autonomous method for condition monitoring of rotating machines during operation based on radio frequency (RF) pulse transmission using energy harvesting from operational vibration. An energy harvesting unit is designed to generate and rectify the energy harvested from the machine vibration using Voltage Multiplier (VM) circuit and to store the energy into a capacitor. Then, this energy harvesting unit runs a smart system consisting of a microcontroller and the RF transmitter designed to send a pulse at specific capacitor voltage. A pulse-based condition monitoring approach is introduced which monitors the state of the machine during the operation. In order to estimate power output of the piezoelectric harvester for a realistic vibration signal, the Fourier Transform concept for signal decomposition is incorporated into the well-known electromechanical distributed parameter model. Using experimental data, performance of this autonomous condition monitoring system is tested for a water pump at different conditions. To do so, acceleration data from a centrifugal water pump are acquired with an accelerometer, which then decomposed into a series of harmonics using Fast Fourier Transform. Then using analytical distribute model, a bimorph energy harvester with two Piezoceramic layers is optimized to generate maximum power from the water pump vibration. Consequently, the condition monitoring of the water pump is performed using the presented pulse-based approach. Results of this study show that, the fault diagnosis can be performed autonomously by applying the pulse-based method presented in this work, and by using the piezoelectric harvesting device as an energy source.

Keywords: Condition Monitoring, Autonomous System, Piezoelectirc Harvesting, Power Management, Fault diagnosis, Water Pump.

1. Introduction

Online condition monitoring (CM) of machines during operation is a key approach for reducing unscheduled downtime and maintenance cost during useful life. CM of rotary machines is one of the most successful and established method using so-called pattern recognition in time or spectra responses [1]. There are vast number of studies for CM using different measurement sensors, which record one response of system during operation, and applying different analyses on the recorded data, such as Fourier or Wavelet transforms. Regarding the connection type for sensors, contact and contactless sensors have been widely practiced for CM of rotating machines. For instance, accelerometer installed on bearing housing [2], accelerometer installed on machine outer case and current sensors on input wires [3], accelerometer installed on bearing housing for shaft [4] and accelerometer on outer case of a water pump [5] were employed for condition monitoring applications. In recent years, to overcome difficulties related to direct instrumentation of rotating components, some researchers applied non-contact sensors for condition monitoring of rotating machines using K-Band Doppler radar [6], laser sensors [7] and vision-based non-projection fringe pattern [8]. Although using contactless sensors

helped the direct instrumentation complexities, these methods still suffer from wiring, instrumentation complexities and battery-related problems.

All the aforementioned approaches used conventional measurement methods which require wiring for sensors to transfer data to a control room. For an industrial plant that includes many rotating machines, the cost of wiring and regular inspection of wires and their connections will be considerable. To eliminate problems in conventional methods, e.g. wiring difficulties, setup implementation and immobility [9], an outline for machine condition monitoring was presented using wireless sensor networks (WSNs) [10]. Although WSNs improved common CM approaches, those that are powered with batteries suffer from short lifetime due to the battery lifespan [11]. In an attempt toward self-powered CM methods, energy harvesting (EH) has emerged as a source of energy for powering batteries in CM applications [11].The energy harvesting has seen a worldwide growing attention in academic and industry during recently [12]. There are various methods to convert often-lost mechanical energy into electrical energy for motor or generator applications, including electromagnetic induction, electrostatic induction and the piezoelectric effect [13]. In the recent years, the number of studies considering energy harvesting for structural health monitoring is rapidly increasing [11]. Energy harvesting by piezoelectric materials provides higher energy density, and can be simply integrated into a system [13], [14].

Recently, smart materials as sensors for system operational condition and structural health monitoring were employed. In some cases, these smart materials also acted as transducers that generate voltage according to the sensed vibration. This concept was used for bridge condition monitoring under forced vibration by adopting piezoelectric energy harvester [15]. In cases, it has been demonstrated that these sensors can provide enough energy for themselves and, hence, can be regarded as self-powered sensors without the need for wiring [16], [17]. Moreover, in some studies, it was shown that a wireless connection can be powered by these self-powered sensors for transferring data or sending a pulse [18], [19]. In the research by Lim et al. [20], piezoelectric patches were installed on wind turbine blades to demonstrate that the patches can provide power for wireless connection from blade strain energy. In the existence of a structural imperfection or a fault in the system, introduced vibration on these smart materials will be different and, hence, this concept can be used for condition monitoring or structural health monitoring. In another study, Lim et al. [21] showed that, by analyzing the time of sending discrete signals between three blades, blade state can be monitored. Patange et al. [22] installed piezoelectric patches onto composite beams in defect-free and delaminated conditions to study output power from these patches under low-frequency vibration excitation. They showed that delaminated beams will generate less energy compared to defect-free ones by demonstrating that the energy

harvesting can be employed for health monitoring. However, they did not assess whether this energy output could be enough for running a self-powered system or how to manipulate output power differences in order to perform health monitoring.

Most of state-of-the-art about fault detection and condition monitoring using smart materials presented only the feasibility of such systems and have not adequately focused on power management and system performance for self-powered condition monitoring. On the other hand, studies that focused on electrical power management for these self-powered systems have not presented appropriate condition monitoring approaches. In addition, in the self-powered condition monitoring systems, the design of vibration energy harvester and related optimization process, as a significant step, has not been addressed. Moreover, most of previous studies about self-powered CM were carried out for structural imperfections such as crack and delamination while there are, apart from the structural faults, some other faults that can occur in an operating machine. One study reported the use of harvested energy from an electromotor for transferring acceleration data through wireless connection [23]. In the presented study, all three essential sections for a vibration-based self-power condition monitoring, namely, the design of energy harvester, power management and condition monitoring approach, are addressed. To the best knowledge of the authors, such a study containing all these areas has not been presented. The presented study uses a new established method based on pulse timing for fault detection of a complex rotating system in conjunction with cantilever piezoelectric beam for generating electrical power, which is easy to integrate in the system. By applying the presented energy harvester and pulse timing method for CM, power and data-transfer wires are no longer necessary. This system can be integrated into an industrial production plant with many rotating machines in a cost effective manner. This study will contribute to the elimination of the need for expensive accelerometers, data acquisition unit with high sampling rate, sensor and equipment, which are typically being used for condition monitoring of high-speed rotary machines.

A robust self-power system is proposed for remote condition monitoring in which elapsed times between RF transmissions are investigated. In this study, experimental data from a real operating water pump is used as self-vibration machine. Then, the vibration signals are considered as base excitation for a piezoelectric harvester beam. Afterwards, using a well-known analytical model based on distributed Euler beam theory, output power from a bimorph with an added tip mass is optimized for maximum power generation from the experimental vibration data. Lastly, a method for remote condition monitoring is established that is relied on pulse-sending times. In this framework, section 2 is dedicated to propose the condition monitoring approach in system level, the conceptual design of energy harvesting unit and pulse-based condition monitoring method. The piezoelectric harvester

contributes to energy harvesting from piezoelectric direct effect. In section 3, the energy harvester model is developed to estimate the output voltage analytically from operational vibration using the Fourier Transform of real vibration signals. Section 4 is dedicated to the experimental test study with a primarily signal processing step for the experimental signals. Finally, results of the applying the proposed condition monitoring on the presented case study is presented in section 5.

2. Autonomous remote condition monitoring

The main objective of this study is to design an autonomous condition monitoring system capable of remote health monitoring for rotating machines during the operation. Therefore, at first, components of the system are selected based on requirements that should be met to achieve online condition monitoring. Then, these components are evaluated regarding power consumption which is followed by an assessment that shows the required energy for the condition monitoring can be provided by the energy harvesting device and, therefore, the system is autonomous. This studs introduces a novel method based on pulse transmission from RF technology for remote condition monitoring. The method relies on comparing the elapsed time between pulses from a continuous operation machine generating vibration during operation. Since vibration is an unavoidable phenomena in operational machines, the focus for energy harvesting in this study is piezoelectric technology as the vibration of machines often contains high frequency harmonics. This section is dedicated to demonstrate such a system in terms of system design, power consumption, energy harvesting unit and pulse condition monitoring approach.

2.1. System Design and Power Consumption

According to the functionality of this novel CM approach, the system should comprise a harvesting unit to generate, rectify and store energy, a low-power microprocessor to control the signal emitting, and RF transmitting unit for sending a binary signal when microprocessor allows. The storage system should always maintain the energy for running microprocessor as well as providing the energy for RF transmitter when it is enabled. Microprocessor can be programmed to power RF circuits when the voltage in the storage reaches to a specific value. This signal transmitting will repeatedly continue after the harvested energy reaches to the defined value each time. If the level of acceleration changes, the harvested energy will be directly influenced and, consequently, the time of RF transmitting is altered. Furthermore, a Failure Index is introduced in this work, which is defined based on the elapsed time between signal transmissions in operation compared to values recorded in defect-free condition. The component in this system are shown in Fig. 1.

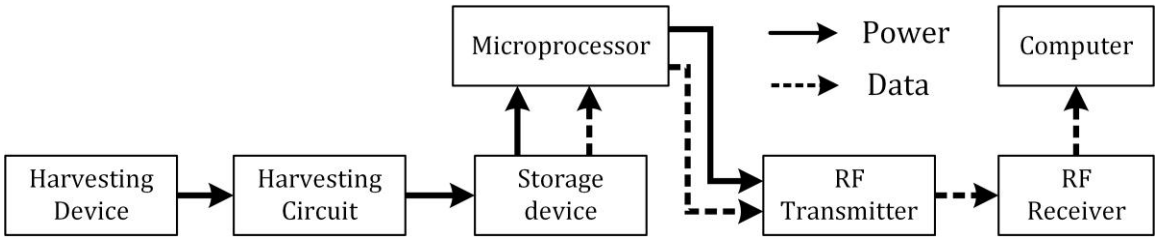

Fig. 1. The protocol for remote condition monitoring

The units in the protocol Fig. 1, which consume energy, are microprocessor and RF transmitter. Among these, the RF transmitter only consumes energy when it is activated by the microprocessor for signal transmitting. On the other hand, the microprocessor needs a permanent energy supply through running. For this reason and to fulfill requirements for this CM method, the microprocessor should have low-power consumption, operate in low voltage, be capable to perform simple calculations and have at least one comparator.

Microchip Technology Inc. [24] is a leading provider of low-power and high-speed flash technology microprocessors, which are appropriate selections for microprocessors in the wireless system design [19], [25]. PIC16F676 as an 8-bit microcontroller is selected for this system because of its low-power consumption, operating at low voltage and very low standby current of 1 nA. It also has 1 comparator and 128 bytes of memory, which makes it suitable for programming with one checking condition. According to [26], this microcontroller consumes 8.5 µA at typical 2.0 V during operating at 32 kHz.

The RF module transmits the data from the Microprocessor when needed. The RF module stands in standby mode for the rest of cycle. The RF module in this work, RTFQ1P [27], is a 9.6 Kbps data transmitter with transmitting range up to 250 m with low-power consumption operating with 3.0 V supply voltage in the standby mode. This RF transmitter consumes 7 mA at 3.3 V voltage supply during the transmission of date and requires a maximum current of 100 nA in the standby mode [27].

2.2. Energy Harvesting Unit

In this study, the piezoelectric based energy harvesting unit is responsible for providing continuous energy to run the microprocessor and RF transmitter request. The harvesting unit consists of an energy harvester, a harvesting circuit and storage system as shown in Fig. 1. The piezoelectric energy harvester is considered as the source of energy production from the machine vibration. The harvester is designed to generate adequate energy to power the remote condition monitoring system. This device should accommodate two critical goals. At first, it should have capability to generate enough electrical energy for continuous operation of the remote condition monitoring system described in subsection 2.1.

Secondly, this device should be designed to be sensitive to occurrence of faults. In many practical cases, the output voltage from the piezoelectric harvester is less than the input voltage required for running the electronic components. In addition, the generated voltage is an A.C. signal while the end-users require D.C. Thus, it is essential to provide a circuit for voltage enhancement as well as converting the A.C. to D.C. In this work, therefore, the energy harvesting circuit provides power supply suitable for the end-users. The capacity of the capacitor in the energy harvesting unit plays an important role in the health monitoring. The energy capacity should be large enough to provide energy in order to guarantee the system operation. On the other hand, since the microprocessor can activate or deactivate the RF transmitter based on voltage level of the capacitor, the capacitor should be small enough to experience a sensible voltage drop due to a short RF transmission. Fig. 2 shows these components in the energy harvesting unit.

There are different types of piezoelectric harvesters and harvester's configuration generally depends to the nature of available load and its frequency. A typical piezoelectric energy harvester as shown in Fig. 2 is made of a bimorph harvester. This bimorph structure is made of a thin substructure shim (usually a metal helping for charge transferring) which is bracketed with two piezoelectric layers. Among piezoelectric harvesters, cantilever configuration is the most widely used option, especially for vibration energy harvesting from mechanical systems [13]. In addition, in some cases an added mass m_a is attached to the end of bimorph for frequency matching. This typical configuration is popular since, in a reasonably small volume, it delivers higher power density [13]. Piezoelectric ceramics have the best piezoelectric characteristics in comparison with the composites and polymers [28]. Among piezoelectric ceramics, PZT is an important material because of its high Curie temperature and excellent energy harvesting potential. It is a well-known fact that piezoelectric harvester generates the maximum voltage when it is excited by an external force with frequency close to its natural frequencies [14]. Generated power from bimorph piezoelectric harvester at resonance is higher than other frequencies even anti-resonance frequency [29]. Hence, in order to scavenge the maximum energy from piezoelectric bimorph, a configuration containing PZT material as the piezoelectric layers should be designed to be excited at its fundamental natural frequency.

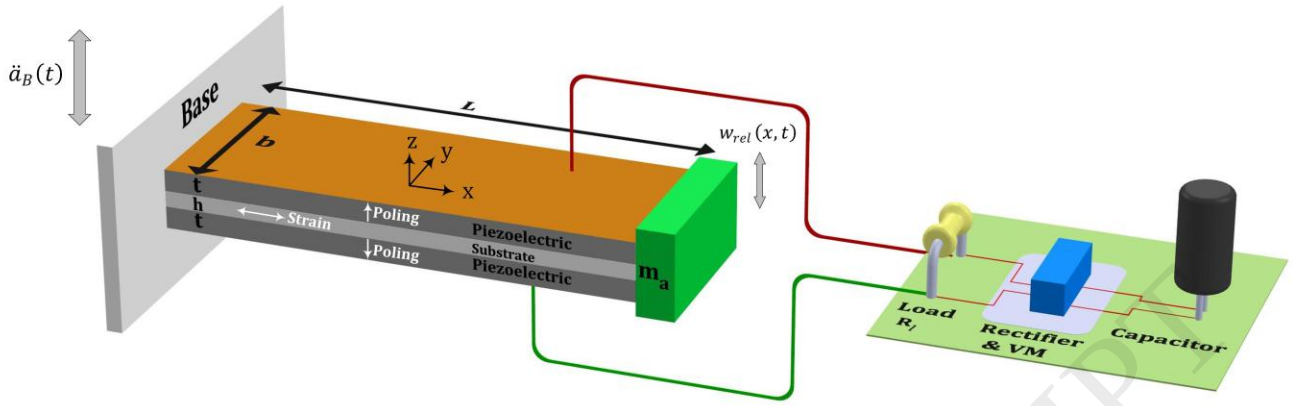

Fig. 2. Energy harvesting unit comprises of piezoelectric bimorph, resistance load, harvesting circuit and capacitor.

One solution for the energy harvesting circuit to increase the voltage and to convert AC to DC is so-called voltage multiplier (VM) or charge pump circuit [30], where a capacitor is charged in one-half of the A.C. input and then discharged into the next circuit section during the second half cycle. Within the framework of VM, Multistage Villard Voltage Multiplier (MVVM) and Multistage Dickson Charge Pump (MDCP) can be used in order to increase the power [31] as have been done by Torah et al. [26] and Galchev et al. [32]. In this study, a MDCP circuit is applied in order to amplify the generated voltage. The MDCP circuit consists of diodes and capacitors, where the stage of MDCP determines the number of diodes and capacitors. In order to obtain the optimum staged of the MDCP, a number of different circuits were compared using MATLAB® Simulink. Siemens BAT760 diodes with a forward bias voltage of ~100mV and current of 0.1 mA were used due to the low forward voltage drop and reverse leak current. For the energy storage, a capacitor with 150 µF was considered in the simulations and the voltage of the capacitor is compromised at different MDCPs in order to obtain the optimum VM circuit. Fig. 3 shows a 5 stage MDCP circuit with BAT760 diodes and the optimum values for the capacitors. The storing output voltage of the capacitors for different MDCP stage circuits and input of 1.85 V at 49.5 Hz are shown in Fig. 4. As can be seen, the 5 stage MDCP delivers the highest voltage output with fast charging time. Therefore, the configuration shown in Fig. 3 is selected as the best design for amplifying the output voltage from the piezoelectric harvester and it is used for the further steps in this study as of the optimized VM configuration.

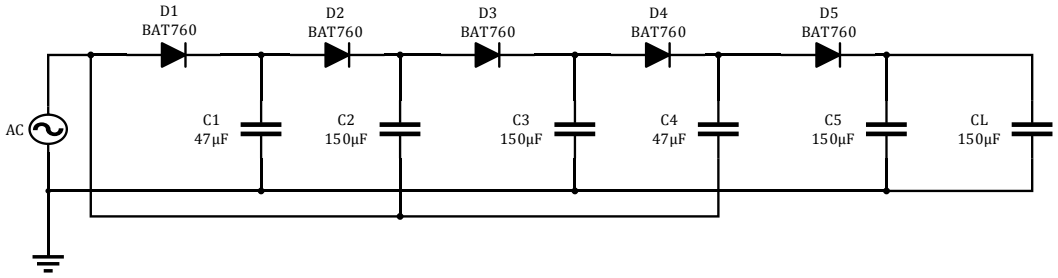

Fig. 3. Optimum 5 stage MDCP circuit for use with the designed piezoelectric harvester

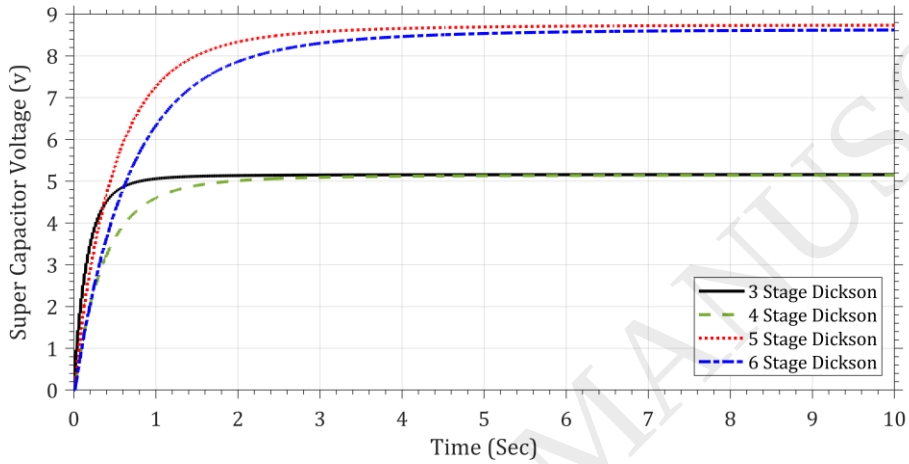

Fig. 4. Storing capacitor voltage outputs for an input magnitude of 1.85 V at 49.5 Hz

2.3. Pulse Condition Monitoring

The presented method relies on the pulse timing method by the RF transmitter for remote condition monitoring. As discussed, the RF transmitter will be enabled by microprocessor to transmit a signal whenever the level of energy in the storage device reaches to the defined value. If the machine is working under normal conditions, no major changes in energy capacitor charging and, consequently, in the RF transmitting processes are expected. Therefore, the pulse timing lies within a band. However, if any fault occurs during machine operation, the immediate change in the acceleration affects the energy storage charging and, consequently, the pulse timing.

Fig. 5 shows the process of condition monitoring based on the pulse timing method. In Fig. 5 (a), the system performance during the normal operation is shown. On top, a typical acceleration of the system is shown. Then, the stored energy is plotted and finally, in the bottom, elapsed time of the pulses are shown versus time. It is worth mentioning that plots do not contain specific values since these figures are presented for showing the concept of this approach rather than focusing on one specific application. When the stored energy reaches to the limit for microprocessor, the microprocessor will be activated

through a voltage-level switch to the circuit. Thus, the energy drops in the stored energy curve. This process is before sending any pulses and is only for the start phase. From this moment the microprocessor is active and tunes the RF transmitting. After the energy in the storage device reaches to an peak value, the microprocessor allows RF transmitter to send the first pulse at time T'. Sending pulses will continue each time after the elapsed time, T, in the regular operation. In Fig. 5 (b), the performance of the system is shown when the fault occurs. The first and second pulses are transmitted after T' and T elapsed times, respectively, just similar to the normal operation. After a specific time, it is assumed that a fault occurred in the machine causing increment in the acceleration and, consequently, the charging process will be faster. Therefore, the elapsed time reduces from normal T to a value of T_d where $T_d < T$. It can be seen that if the fault occurred during one of the charging phases, the elapsed time is not equal to T nor T_d as the capacitor has not been charged in none of healthy and damage conditions. This charging phase is called transient interval and its elapsed time is denoted with T_{tr}, where $T_d < T_{tr} < T$. This transition phase is an indicator that machine state is being changed. It is worthy to note fast charging of capacitor at abnormal condition.

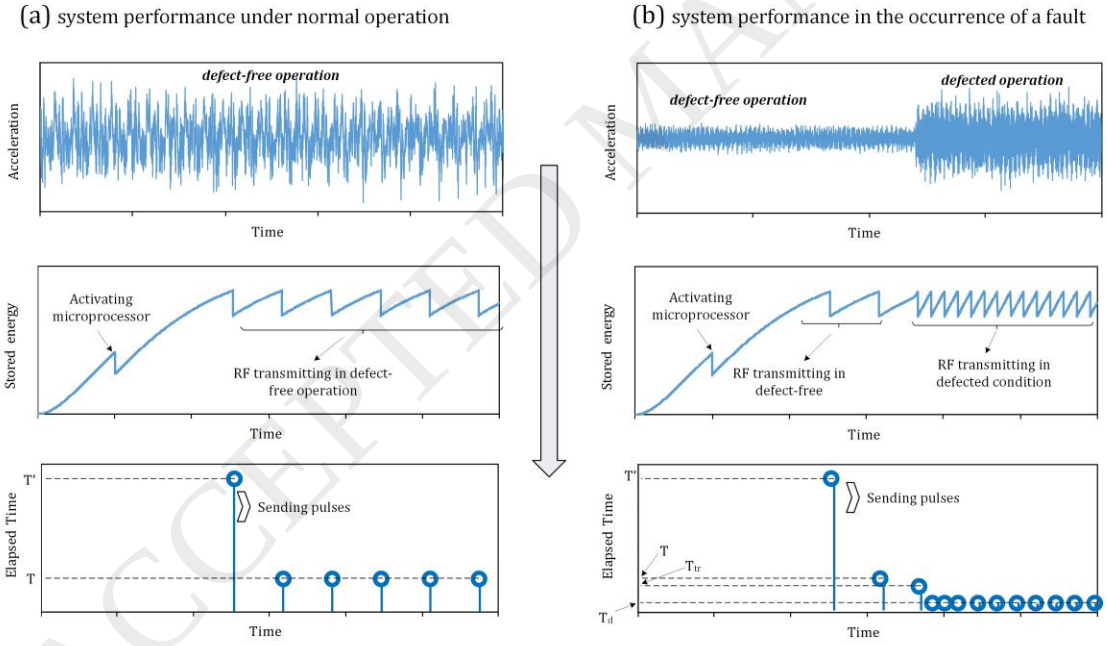

Fig. 5. Condition monitoring based on pulse timing method

One important assessment in this method is the statistical analysis of elapsed time as obviously the elapsed time of the pulses undergoes minor differences due to the nature of experimental errors. The elapsed time between the pulses can be modeled as:

$$T_{ij} = \mu + \tau_i + \epsilon_{ij} \qquad i = 1, \dots, N_{cnd}\,, j = 1, \dots\,, N_{exp} \tag{1}$$

where μ is the average of elapsed times in defect-free condition, τ_i is the effect of machine condition on the elapsed time, ϵ_{ij} are the experimental errors, N_{cnd} is the number of conditions considered and N_{exp} is the maximum number of elapsed time figures obtained experimentally for different conditions of the machine. The experimental errors are independent and normally distributed due to randomness of experiments, e.g. $\epsilon_{ij} \sim N(0, \sigma_i^2)$, where σ_i is the standard deviation of errors. It is worth mentioning that $i = 1$ is the defect-free condition while $i > 1$ corresponds to faulty conditions. Based on these definitions, $\tau_1 = 0$ while $\tau_{i>1} \neq 0$.

Now, the pulse condition monitoring can be performed as follows:

Step 1: A set of data from the machine at different working conditions including defect-free state is formed and then one should be able to compute the statistical features in Eq. (1), e.g. μ, τ_i and σ_i.

Step 2: After each pulse transmission, the elapsed time, called $\hat{\mathrm{T}}$, between the current pulse and previous pulse should be computed.

Step 3: Fault Index (FI) is defined as:

$$\mathrm{FI} = \left(\hat{T}/\mu - 1\right)^2 \tag{2}$$

FI is in the range of 0 to 1, where 0 means the machine is in defect-free condition while 1 means that the machine works abnormally. In addition, a considerable change in the FI identifies a change in the machine state. This FI has a confident limit (CL) of:

$$\mathrm{CL} = 1 - \mathcal{D}_{\hbar}/\mu + \tau_{\hbar} \tag{3}$$

where $\mathcal{D}_{\hbar}$ is the distance between elapsed time $\hat{T}$ and the average of elapsed time in $\hbar$-th machine condition. In addition, $\hbar$ is the class in which $\mathcal{D}_{\hbar} = \left|\hat{T} - (\mu + \tau_{\hbar})\right|$ is minimum. By this definition, CL is the certainty of FI, which demonstrates assurance of the identified machine condition. The higher CL is, the more reliable the machine condition monitored.

Step 4: In order to detect type of the fault, a state parameter can be defined as $\mathcal{S}$:

$$\Gamma_{\mathcal{S}} = min\left\{\left(\frac{\hat{T}}{\mu+\tau_{\mathcal{S}}} - 1\right)^2\right\} \tag{4}$$

If $\mathcal{S}$ is equal to 1, the state of machine is normal, otherwise $\mathcal{S}$ is the class of defined fault.

In order to show the performance of this CM method, a situation is considered in which the state of a machine changes from "1" to "2" and then to "3". State "2" has lower elapsed transmission time while elapsed transmission time of "3" is higher than "1". Fig. 6 (a) shows the considered elapsed time between the transmissions over time. Based on these values, the FI and machine state $\mathcal{S}$ are calculated

using Eq. (2) and (4), respectively and graphically shown in Fig. 6 (b). As shown, the FI is close to 0 until the elapsed time is within the range of "1" state. After the system state changed to "2", $\mathcal{S}$ jumped to 2 and FI is no longer close to 0. Finally, in the second change of system state to "3", $\mathcal{S}$ remains at 3 and a change in the FI scatter can be observed. Although this is a numerical example of the pulse system performance, it shows that in the both cases whether the elapsed time is lower or higher than the standard elapsed time, this method can predict state of the machine and the FI value can be an accurate indicator of the state.

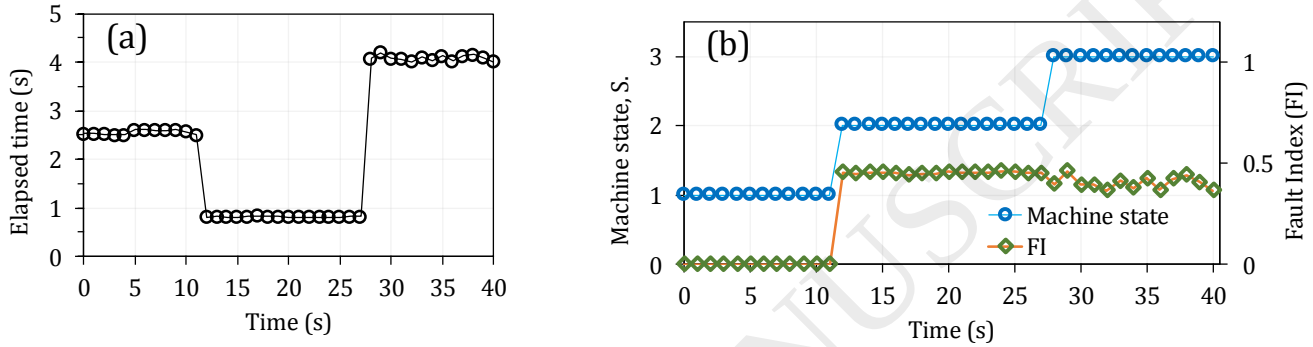

Fig. 6. An example for pulse condition monitoring, (a) Elapsed transmission time and (b) FI and machine state

3. Modeling of Piezoelectric Energy Harvesting Device

This work will model the piezoelectric bimorph harvester with electromechanical distributed parameter model in which the bimorph harvester is considered as a uniform beam with Euler-Bernoulli beam assumptions according to the study by Erturk and Inman [33]. A perfect bonding between substructure and piezoelectric layers are considered. Moreover, it is assumed that the piezoelectric layers are covered with negligible thickness continuous electrode layers and are connected in series. In this study, it is assumed that the base displacement induced from the machine operation is only defined by translation and not rotation as the vibration is in translation form. However, if rotation plays an important role in base excitation, its effect can be added to the equations but here only translational base excitation is considered.

As shown in Fig. 2, the base acceleration expressed with $\ddot{a}_B(t)$ causes a relative transverse deflection of the beam to its base at location x and time t shown with $w_{rel}(x,t)$. it is of interest to define $w_{rel}(x,t)$ with modal expansion such as:

$$w_{rel}(x,t) = \sum_{i=1}^{\infty} \phi_i(x)\,\eta_i(t) \tag{5}$$

where $\phi_i(x)$ is the beam mode shapes of the i-th vibration mode and $\eta_i(t)$ is the mechanical response in modal coordinates. For the clamped-free boundary conditions, beam mode shapes is given by Eq. (6) [34]:

$$\phi_i(x) = \chi_i[cosh\lambda_i x - cos\lambda_i x + \alpha_i(sinh\lambda_i x - sin\lambda_i x)] \quad (6)$$

where α_i is a constant given by Eq. (7) and χ_i is a constant for satisfying mass normalization of the mode shapes, e.g. $\int_0^l m^* \phi_i^2(x)\,dx + m_a \phi_i^2(L) = 1$.

$$\alpha_i = \frac{\sin\lambda_i - \sinh\lambda_i + \lambda_i \frac{m_a}{m^* L}[\cos\lambda_i - \cosh\lambda_i]}{\cos\lambda_i + \cosh\lambda_i - \lambda_i \frac{m_a}{m^* L}[\sin\lambda_i - \sinh\lambda_i]} \quad (7)$$

With the modal expansion defined and applying the modal orthogonality conditions, the electromechanical coupling equations can be expressed with:

$$\ddot{\eta}_i(t) + 2\zeta_i \hat{\omega}_i \dot{\eta}_i(t) + \omega_i^2 \eta_i(t) + \Upsilon_i V_P(t) = f_i(t)$$

$$C_P \dot{V}_P(t) + (1/R_l)V_P(t) = \sum_{j=1}^{\infty} \Lambda_i \dot{\eta}_i(t) \quad (8)$$

where $\hat{\omega}_i$ is the undamped natural frequency of the beam in short circuit condition expressed with Eq. (9), ζ_i is the mechanical damping ratio, $f_i(t)$ is the modal mechanical force given by Eq. (10), C_P is the internal capacitance given by Eq. (11) as a function of relative permittivity $\bar{\varepsilon}_{33}$ and piezoelectric layer geometry, Υ_i is the modal electromechanical term defined by Eq. (12) and Λ_i is the modal electrical coupling term expressed in Eq. (13):

$$\hat{\omega}_i = (\lambda_i l)^2 \sqrt{YI/m^* L^4} \quad (9)$$

$$f_i(t) = -m^* a_B(t)\left[\int_0^L \phi_i(x)dx + m_a \phi_i(L)\right] \quad (10)$$

$$C_P = \bar{\varepsilon}_{33} bL/t \quad (11)$$

$$\Upsilon_i = \frac{\bar{e}_{31} b}{2t}\left[h^2/4 - \left(t + h/2\right)^2\right].\frac{d\phi_i(x)}{dx}\Big|_{x=L} \quad (12)$$

$$\Lambda_i = -\frac{\bar{e}_{31}(t+h)b}{2}.\frac{d\phi_i(x)}{dx}\Big|_{x=L} \quad (13)$$

In Eq. (9) λ_i is the characteristic number shown obtained from solving Eq. (14), $\bar{e}_{31}$ is piezoelectric constant in 31 mode and $\bar{\varepsilon}_{33}$ is the permittivity constant. Also, m^* is the unit mass per length and EI is the bending stiffness given by Eq. (15) [33].

$$1 + \cos\lambda_i \cosh\lambda_i + \lambda_i \frac{m_a}{m^* L}(\cos\lambda_i \sinh\lambda_i - \sin\lambda_i \cosh\lambda_i) = 0 \quad (14)$$

$$YI = {}^{2b}/_{3}\left[Y_s\, {}^{h^3}/_{8} + \bar{c}_{11}^{E}\left(\left(t + {}^{h}/_{2}\right)^3 - {}^{h^3}/_{8}\right)\right] \quad (15)$$

where Y_s is the Young's modulus of substrate layer and $\bar{c}_{11}^{E}$ is the stiffness of piezoelectric material at constant electrical field.

If $\ddot{a}_B$ is presented with a series of harmonic functions using the Fourier Transform, Eq.(20), then by defining the sampled frequency with $\omega_k = \frac{2\pi k}{N}$, the force term becomes $f_i(t) = \sum_{k=0}^{N-1} F_i(\omega_k) e^{+\mathrm{j}\,\omega_k t}$, where $F_i(\omega_k)$ is expressed as follows:

$$F_i(\omega_k) = -m^*\left(\frac{1}{N}\left|\ddot{A}(\omega_k)\right|\right)\left[\int_0^L \phi_i(x)dx + m_a\phi_i(L)\right] \quad (16)$$

By this harmonic representation of base excitation and superimpose characteristic for linear systems, the resulting complex voltage amplitude is also a series of harmonic functions shown as:

$$V_P(t) = \sum_{k=0}^{N-1} \bar{V}_P(\omega_k)\, e^{+j\,\omega_k t} \quad (17)$$

where $\bar{V}_P(\omega)$ is the magnitude of output voltage corresponding to each frequency. By substituting Eq. (16) and (17), the steady state voltage response can be shown as:

$$V_P(t) = \sum_{k=0}^{N-1} \frac{\sum_{i=1}^{\infty} \frac{j\omega_k \Lambda_i F_i(\omega_k)}{\hat{\omega}_i^2 - \omega_k^2 + j2\zeta_i\omega_k\hat{\omega}_i}}{\frac{1}{R_l} + j\omega_k \frac{C_P}{2} + \sum_{i=1}^{\infty} \frac{j\omega_k \Lambda_i Y_i}{\hat{\omega}_i^2 - \omega_k^2 + j2\zeta_i\omega_k\hat{\omega}_i}} e^{+j\,\omega_k t} \quad (18)$$

Using the calculated voltage from Eq. (18), the magnitude of output power from piezoelectric harvester can be calculated as $P_p = {}^{|V_p|^2}/_{R_l}$.

4. Experimental procedure and primarily signal processing

For the tests, a centrifugal pump with five vanes connected to an electromotor was equipped with an accelerometer type VMI-102, as shown in Fig. 7. Vibration signals in time-domain were directly measured from the water pump working under different conditions at a constant rotation speed of 2970 rpm. The accelerometer has a sensitivity of 100 mV/g and a resonant frequency of 30 kHz, was mounted vertically on the water pump body.

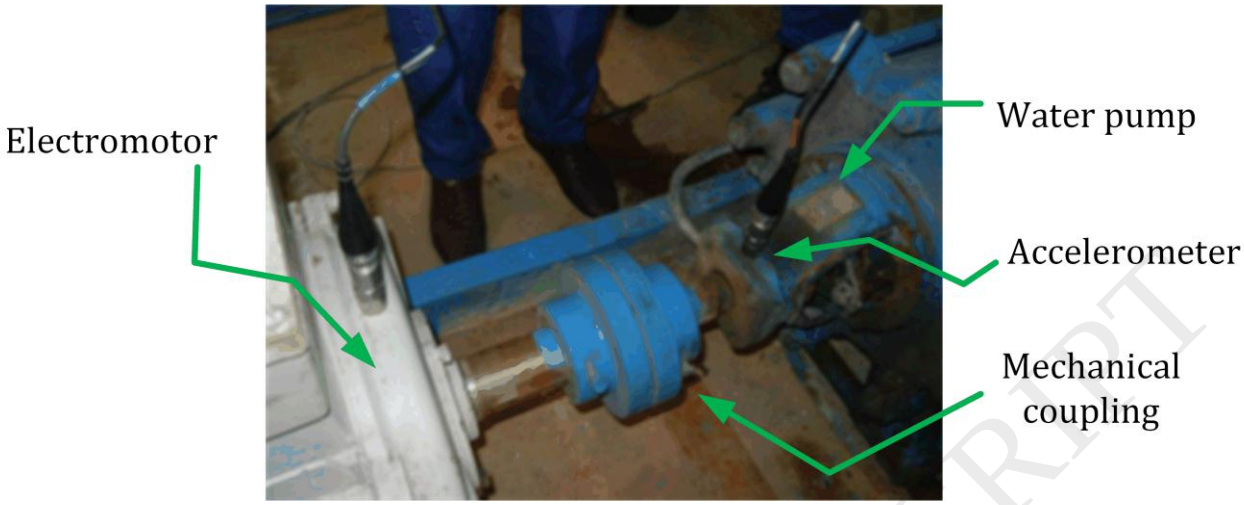

Fig. 7. The water pump connected to the accelerometer

The accelerometer was connected to the signal conditioning unit (X-Viber FFT analyzer), where the signal goes through a charge amplifier. The software SpectraPro-4, which accompanies with the signal conditioning unit, was used for recording the signals directly in the computer. The vibration signal for each pump condition was acquired with an 8192-Hz sampling frequency at a duration of 100 s. Each vibration signal was segmented into 50 smaller vibration signals called data samples. Therefore, each data sample included a 2-s vibration signal with 16,384 data points. Each data sample was then transferred into frequency-domain by FFT method.

Acceleration data in time domain from water pump in healthy, shaft misalignment and shaft looseness conditions are shown in Fig. 8. A rough look into these signals reveals that the amplitude of the acceleration is different when water pump is working in faulty conditions. Shaft looseness and misalignment enhanced the acceleration sensed by the sensor, from a maximum of 8.11 ms^{-2} in defect-free condition to 13.00 ms^{-2} and 27.44 ms^{-2}, respectively. It can also note that not only the maximum acceleration was increased by the faults, the dispersion of the data increased from $\sigma = 2.51\ m.s^{-2}$ in defect-free condition to $\sigma = 7.47\ m.s^{-2}$ for shaft misalignment and $\sigma = 3.72\ m.s^{-2}$for shaft looseness conditions too.

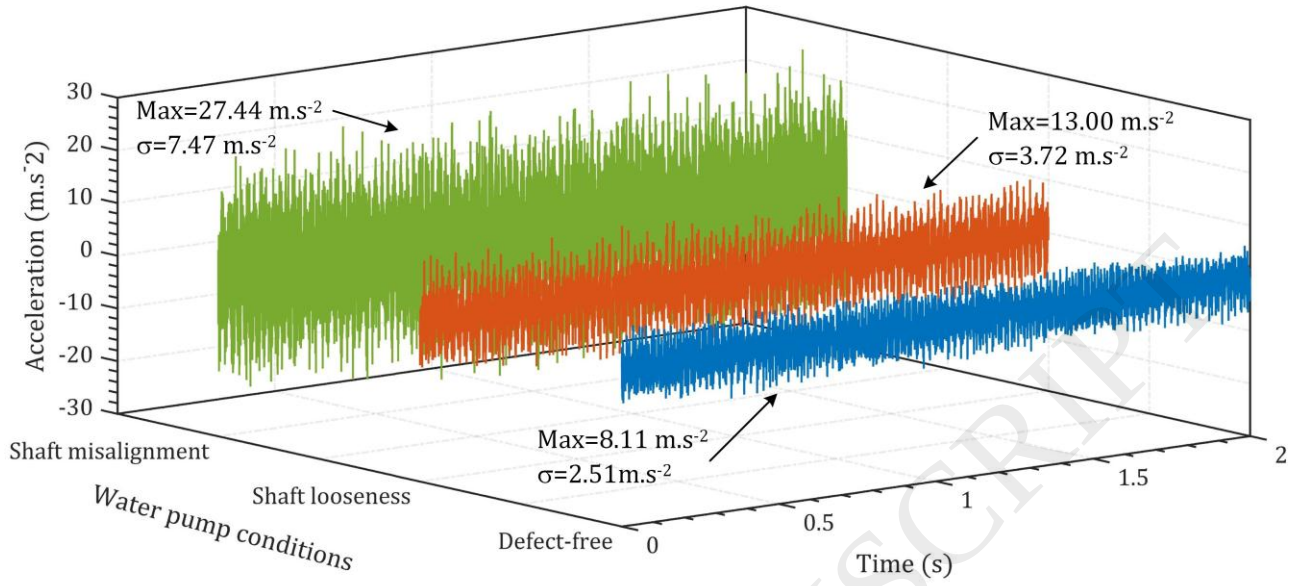

Fig. 8. Time signals of the water pump in defect-free, shaft looseness and shaft misalignment conditions

In this work, a primary signal processing using the Fourier Transform is performed for two reasons. Firstly, frequency matching between fundamental frequency of the harvester and vibration source is essential for designing the harvester. Second, in order to demonstrate which frequency from the vibration source is more sensitive to the faults, amplitude of the Fourier Transform coefficients at dominant frequencies was compared. Since each acceleration signal is a finite sequence of the data, Discrete Fourier Transform (DFT) was applied. If $\ddot{a}(t)$ is the acceleration data which is defined at N time sequences, DFT $\ddot{\mathrm{A}}(\omega)$ and inverse of DFT $\ddot{a}(k)$ are defined by Eq. (19) and Eq. (20), respectively [35]:

$$\ddot{\mathrm{A}}(\omega) = \sum_{k=0}^{N-1} \ddot{a}(k)\, e^{-j\frac{2\pi}{N}\omega k} \tag{19}$$

$$\ddot{a}(k) = \frac{1}{N}\sum_{\omega=0}^{N-1} \ddot{\mathrm{A}}(\omega)\, e^{+j\frac{2\pi}{N}\omega k} \tag{20}$$

Note that $\ddot{\mathrm{A}}(\omega)$ is complex while $\ddot{a}(k)$ is real. From the inverse DFT and Euler formula for complex numbers, the contribution of $\ddot{a}(k)$ from $\ddot{\mathrm{A}}(\omega)$ is expressed as:

$$\ddot{a}_{\omega}(k) = \frac{1}{N}\left|\ddot{\mathrm{A}}(\omega)\right| e^{+j\frac{2\pi}{N}\omega_k} = \frac{1}{N}\left|\ddot{\mathrm{A}}(\omega)\right| sin\left(\frac{2\pi}{N}\omega k + \frac{\pi}{2} + Arg\{\ddot{\mathrm{A}}(\omega)\}\right) \tag{21}$$

Fast Fourier Transform (FFT) is a fast numerical method to apply DFT on signals [35]. FFT of acceleration signals from the water pump at different working conditions are extracted by MATLAB®

and are shown in Fig. 9. To carefully consider frequencies of interest and for better view, a detailed view of FFT signals in 0-500 Hz range is plotted in dB scale. Working under normal condition, the water pump response has dominant frequencies of 49.5 Hz, 100.0 Hz, 148.0 Hz, 197.5 Hz, etc. These frequencies are the 1X, 2X, 3X, and 4X frequencies of the water pump. When water pump is working under faulty conditions, either shaft looseness or misalignment faults, dominant frequencies experience no change in 1X and a minor change in 2X.

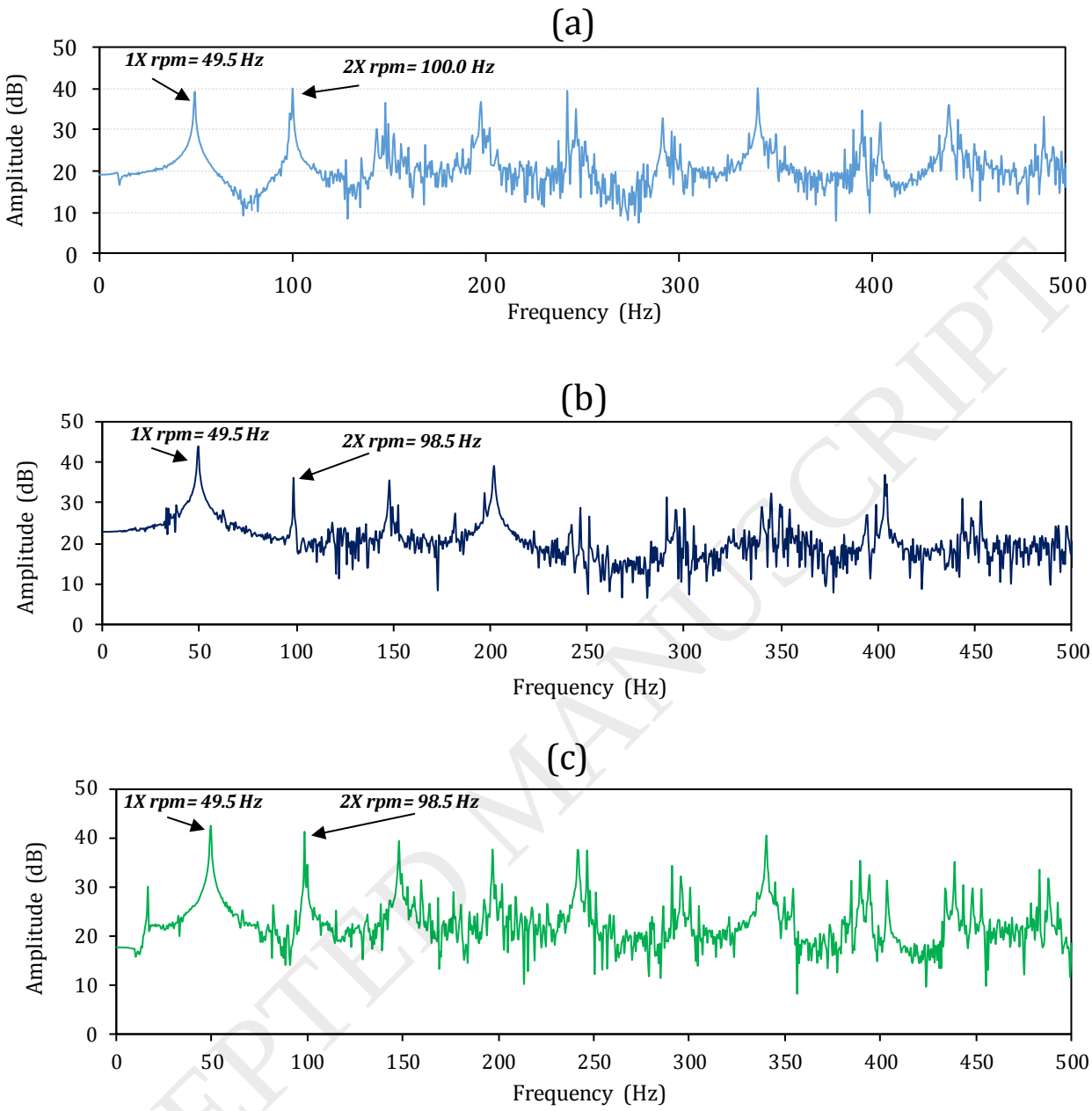

Fig. 9. Fast Fourier Transform (FFT) of time signals from water pump at different conditions with focus on 0-500 Hz range (a) defect-free, (b) shaft misalignment, and (c) shaft looseness conditions

By applying Eq. (21) on the FFT signals, contribution of the eight dominant frequencies in the pump acceleration signals at different working conditions is shown in Fig. 10. Unlike the resonant frequencies which slightly changed, the contribution of the frequencies in the acceleration signals varied considerably for different conditions. The contribution of 1X frequency 49.5 Hz in the shaft misalignment and looseness conditions are 1.04 and 1.49 $m.s^{-2}$, respectively, which are considerably higher than 0.49 $m.s^{-2}$ for the defect-free condition. However, the mode contribution is not always

higher in defected conditions. For instance, contribution of 2X frequency in shaft misalignment is less than the value for the defect-free and shaft looseness conditions.

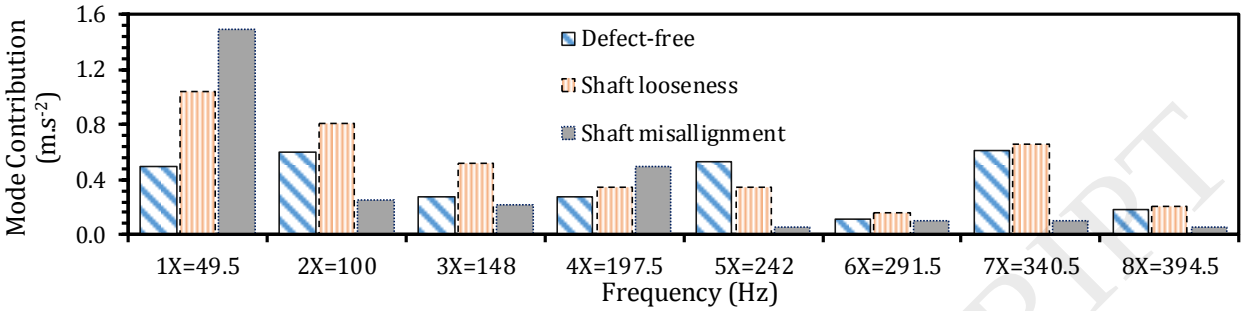

Fig. 10. Contribution of the eight dominant frequencies of the water pump acceleration at different working conditions

5. Condition Monitoring Results and Discussion

For presenting the condition monitoring results for the water pump based on the designed system in section 2, the acceleration data from the experiments, presented in section 4, is used as the base excitation for piezoelectric beam. The piezoelectric beam is connected to the outer case of the water pump with a solid plate, so the piezoelectric beam will be excited from the clamped end with acceleration signal measured experimentally. Fig. 11 shows a schematic of energy harvester attached to the water pump. Afterwards, output power are estimated analytically by using the distributed beam model with the measured base excitation signal at different pump conditions. Lastly, the state of the water pump is monitored by applying the pulse-timing based method. Piezoelectric beam optimization is performed with COMSOL®. All other numerical simulations, including the output power estimation, voltage multiplier simulation and pulse-timing method are carried out with MATLAB®.

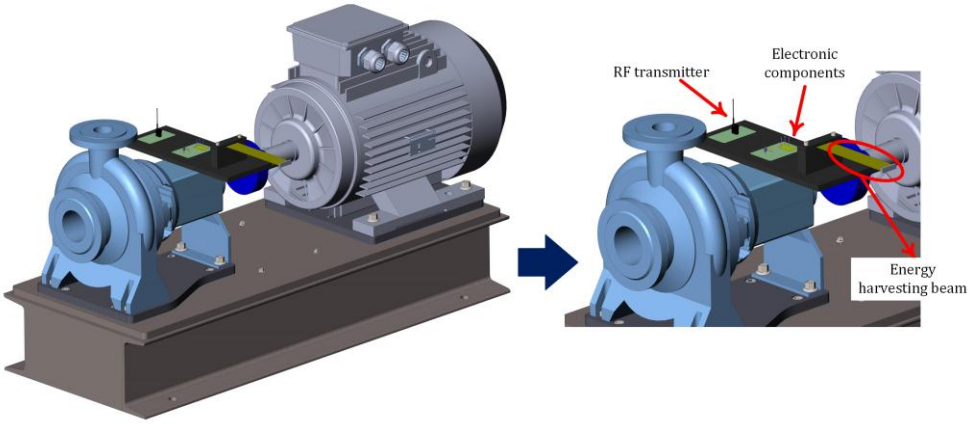

Fig. 11. A schematic of possible assembling of the proposed system into outer case of the water pump

Piezoelectric bimorph generates the maximum power when vibrates at its resonance. Since the power generation has a square factor of magnitude of the excitation acceleration [36], it is preferable that this frequency has a high mode contribution. Furthermore, in order to satisfy the criteria for condition monitoring, the contribution of this frequency should vary noticeably with respect to water pump condition. Thus, optimal design of the piezoelectric harvester has a fundamental frequency close to one of the dominant frequencies in the water pump acceleration signals. By considering these guidelines and analyzing Fig. 10, the 1X frequency is selected as the fundamental frequency of the piezoelectric harvester since the contribution of the frequency 49.5 Hz is high at every working condition and is, moreover, sensitive to the pump working conditions.

Maximum power from piezoelectric harvester is obtained when optimum load resistance is connected and the harvester natural frequency matches to excitation frequency. In this research, with the bimorph topology shown in Fig. 2 and PZT-5A as selected piezoelectric material, the optimization process for frequency matching was proceeded. Afterwards, using analytical modeling approach in section 3, optimum load resistance was selected. Piezoelectric harvesters are available in different geometries and therefore the optimization can be performed for any combination of these geometric parameters, such as length or thickness. In order to narrow down optimization factors, a commercial piezoelectric harvester with low natural frequency from Piezo Systems Inc. (T226-A4-503X) was selected and then by tuning the added mass, frequency matching was performed to match the fundamental natural frequency of the harvester to 49.5 Hz from the water pump acceleration. This piezoelectric sample have been previously used for energy harvesting by [33], [37]. The bimorph sample consists of two oppositely polled PZT-5A layers embracing a brass substrate, representing

series connection between the piezoelectric elements. Geometric and material properties of this samples is presented in Table 1.

Table 1. Material properties of bimorph piezoelectric energy harvester (T226-A4-503X)

Properties	Values
Piezoelectric stiffness at constant field, c_{11}^{E}, GPa	66.0
Piezoelectric density, ρ_p, kg/m^3	7750
Electromechanical coupling coefficient, e_{31}, C/m^2	-14
Piezoelectric layer thickness (each), t, mm	0.26
Piezoelectric permittivity constant, $\bar{\varepsilon}_{33}$, F/m	1800×ε_0
Substrate Young's modulus, Y_s, GPa	105
Substrate thickness, h, mm	0.14
Substrate density, kg/m^3	9000
Device length (active length as clamped), L, mm	55
Device width, b, mm	31.8

To optimize the energy harvester, an objective function is defined as the square of difference between the fundamental natural frequency of the harvester, which is a function of added mass, and frequency of 49.5 Hz as the excitation frequency from the water pump. The objective function shown by Eq. (22) is employed to find the value of m_a by minimizing the objective function.

$$\Gamma(m_a) = (\widehat{\omega}_1(m_a) - 49.5)^2 \tag{22}$$

Fig. 12 (a), (b) and (c) show the error versus iteration number, objective function and the variation of the harvester first natural frequency with respect to the added mass, respectively. Objective function in Fig. 12 (b) shows that, with an added mass of 7.3≤ m_a ≤8.5 g, the objective function is less than 2.5, which is equal to 3% error. As can be seen from Fig. 12 (c), with an added mass of 8 g, the fundamental natural frequency of the harvester matches to 49.5 Hz. For structural steel with the density of 7850 kg/m^3 for the added mass, 8 g will be equal to a solid block with 4×31.8×8 mm dimensions. Hence, the volume of the energy harvester, including the piezoelectric sheets, substrate layer and tip added mass, are 2.15 cm^3. The added mass block can be connected to the piezoelectric sheet with an adhesive connection by an epoxy. For stronger connection, it is recommend to cut a groove in the added mass in order to insert the sheet and fill the gap with the epoxy. Fig. 13 shows added mass features, e.g. material and dimensions, and its connection to the piezoelectric sheet.

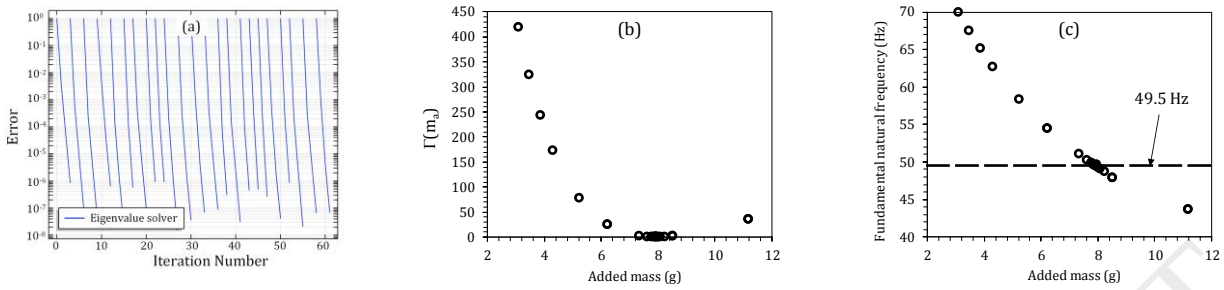

Fig. 12. (a) Convergence history of optimization, (b) objective function (c) the effect of added mass on the harvester fundamental natural frequency

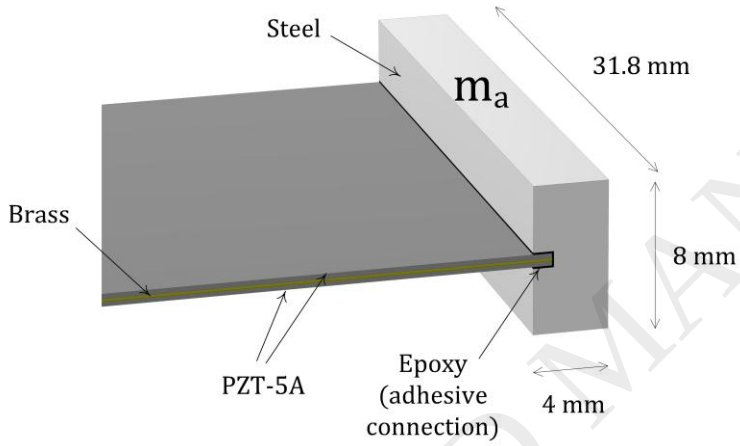

Fig. 13. Detail view of harvester beam with dimensions of the added mass and its connection to the piezoelectric sheet

An analytical modal analysis was performed for this designed bimorph configuration with 8 g added mass and the results are shown in Fig. 14. It can be seen that the first natural frequency of the beam is 49.5 Hz. Moreover Fig. 14 shows that, the other natural frequencies do not match with the operational working frequencies of the water pump. Hence, the contribution of other working frequencies, e.g. 2X, 4X, is negligible. Therefore, in Eq. (18), $\omega_k = 49.5\ Hz$.

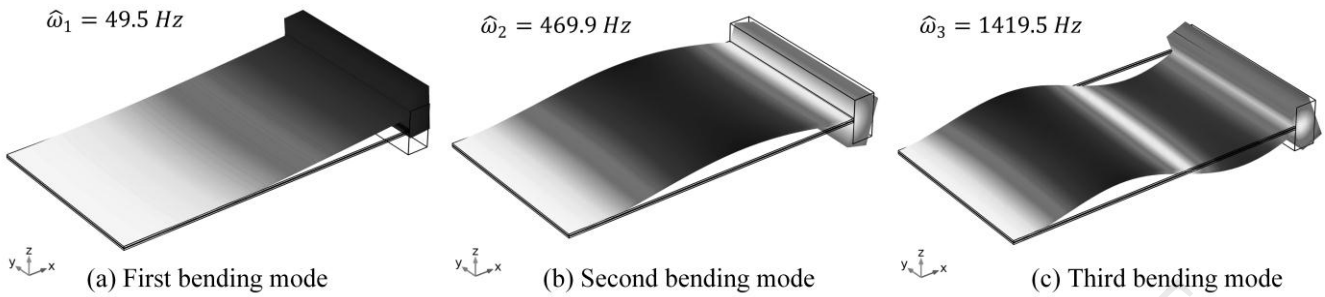

Fig. 14. The first three bending modes for the optimum bimorph harvester

The next step in the design of piezoelectric harvester is selection of load resistance R_l in order to obtain the maximum power. The output voltage and power, considering a unit excitation magnitude of 1 m/s^2 using Eq. (18), are plotted in Fig. 15 (a) and (b), respectively, for different resistance loads. As shown, by increasing R_l, the voltage continuously increases while the output power decreases when the applied load resistance is higher than the optimal resistance. In addition, resonance frequency is slightly changed by increasing the load resistance due to the back piezoelectric effects. To find the optimum R_l, output power curves at resonance and at 49.5 Hz are shown versus the load resistance in Fig. 15 (c). Since the resonant frequency experiences a small change due to increment of the load resistance, the power plots separate after a specific load resistance. The resonant output power is higher than the power at 49.5 Hz, but power at 49.5 Hz is of interest because of the dominant frequency of the water pump vibration. The maximum power is 320 μW/m^2.s^{-4} at 49.5 Hz at load resistance $(R_l)_{opt}$ equals to 44.6 kΩ.

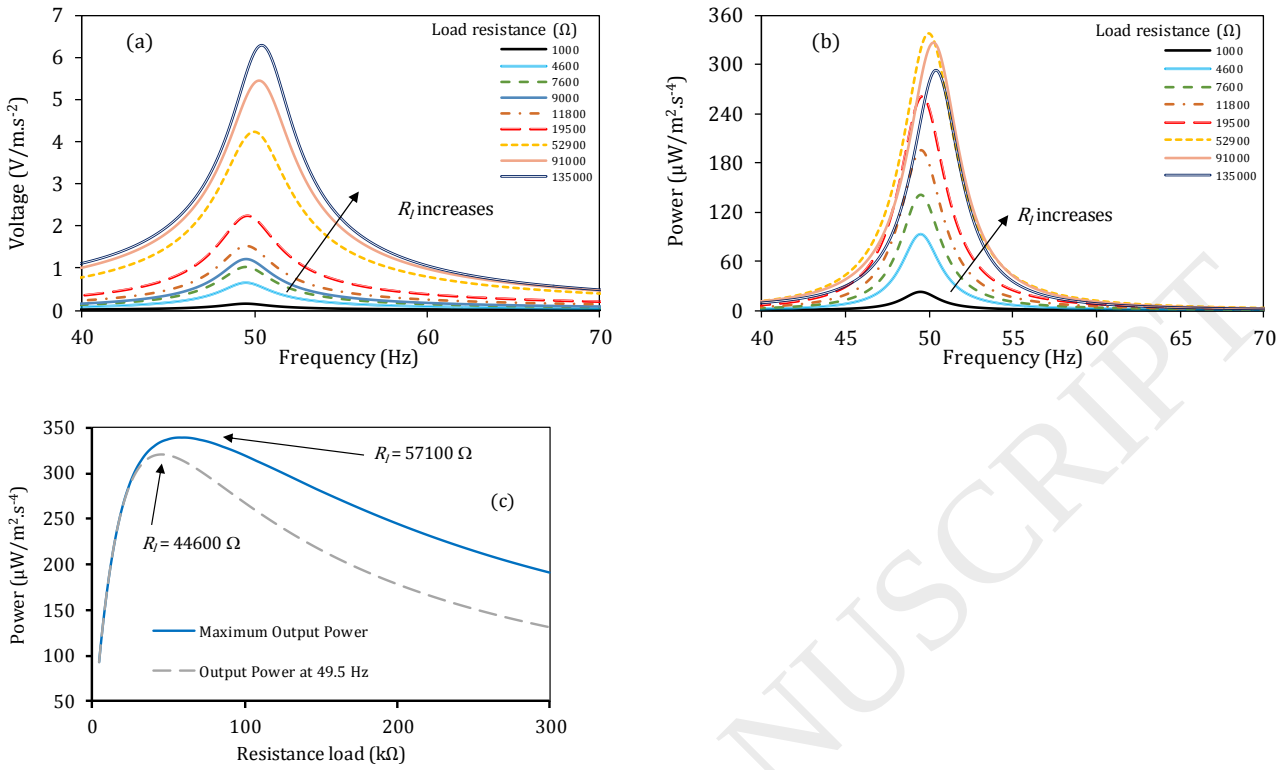

Fig. 15. (a) Voltage and (b) power for different resistance loads versus frequency (c) power for resistance loads at resonance

If the designed harvester is attached on the accelerometer location, as shown in Fig. 11, the measured vibration shown in Fig. 8 can be applied as the base excitation for the harvester. Acceleration in theory is a summation of indefinite number of harmonic functions. In practice, the acceleration signal can be decomposed into a series of defined harmonic functions, as shown in section 4, where the FFT is employed for decomposing the signal into harmonic functions. However, since piezoelectric energy harvesters generate the maximum power at its resonant frequency and the designed harvester has a natural frequency of 49.5 Hz, the significant harmonic in the water pump acceleration is the main dominant frequency, e.g. 1X=49.5 Hz. According to Fig. 10, the magnitudes of 1X harmonic in the water pump acceleration are 0.49, 1.04 and 1.49 m.s^{-2} in defect-free, looseness conditions and shaft misalignment, respectively. Using these figures as the input acceleration, one can calculate output voltage and power for the optimum load resistance. Fig. 16 (a) and (b) show the output voltage and power from one bimorph harvester over a frequency range. As stated, the important figure for the output voltage and power is that of frequency 49.5 Hz, which is plotted for different water pump conditions. The output peak-to-peak voltages from the water pump acceleration at the optimum load are 1.85, 3.93 and 5.63 V at defect-free, shaft looseness and shaft misalignment conditions,

respectively. The corresponding powers are 76.84, 343.12 and 710.45 µW, respectively. If the power density per device volume is divided into square of the input acceleration, power density per square acceleration is 30.8 mW/cm^3.g^2 in all operating conditions. The results does not depend to the input acceleration and is only a function of geometries of the piezoelectric harvester and its material. The voltage and power densities per device volume for different working conditions are shown in Fig. 16 (c). The power density values are equal to 35.7, 160.99 and 330.4 µW/cm^3 for defect-free, shaft looseness and misalignment, respectively. Therefore, the power density is increased by 350% and 824% due to presence of the shaft looseness and shaft misalignment, respectively. This high variation of the power density proves that the storage capacitor will be charged faster in the faulty working condition.

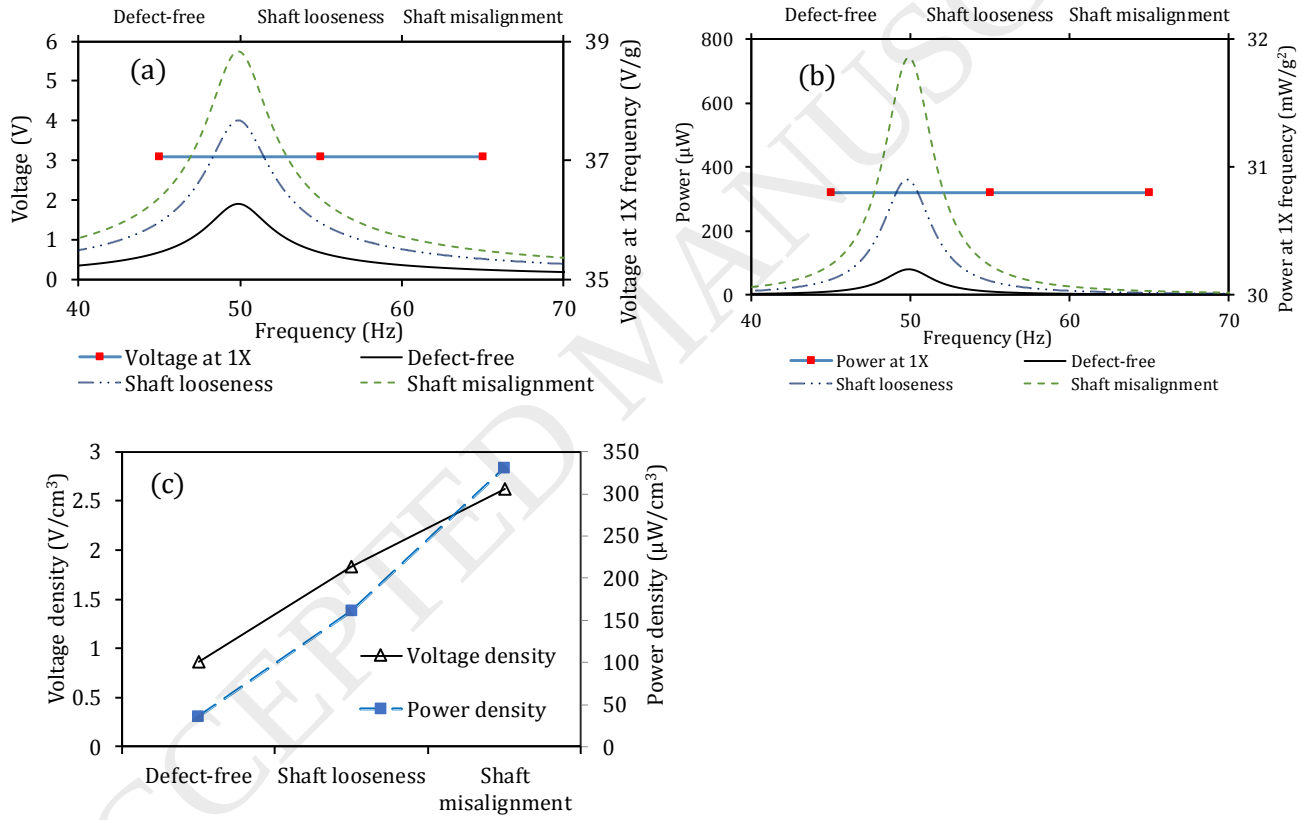

Fig. 16. (a) Voltage, (b) power from water pump acceleration versus frequency and (c) voltage and power densities from the water pump acceleration at 49.5 Hz

Using the optimum VM configuration with 150 µF capacitor, the stored energy in the capacitor from the water pump vibration was calculated. Since the pump acceleration is different at different working conditions, the generated voltage and, hence, the stored energy in the super capacitor are not similar. Fig. 17 shows voltage in the storage capacitor for various water pump conditions. As expected, the

voltage is distinctively higher in both shaft misalignment and looseness than the voltage in defect-free condition. Moreover, the capacitor voltage is significantly higher for the shaft misalignment compared to the looseness condition.

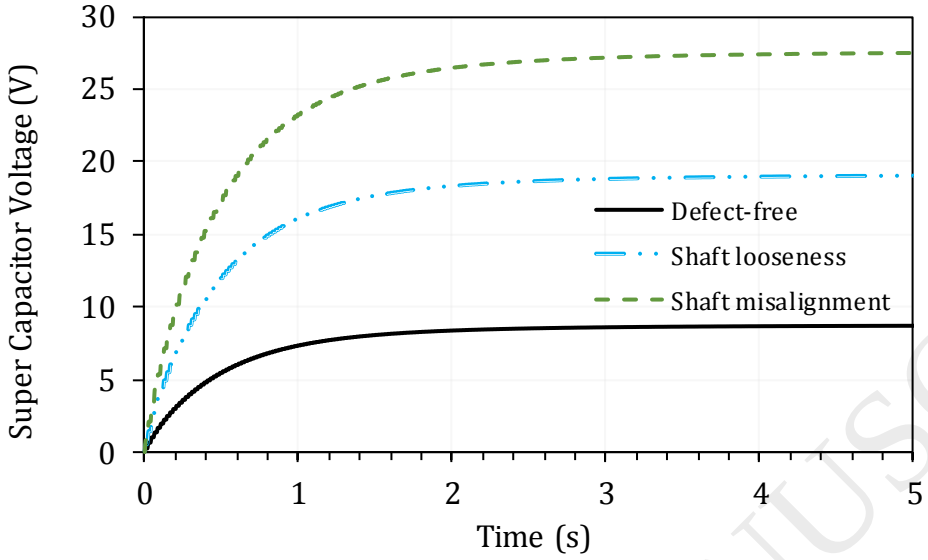

Fig. 17. Voltage outputs in the capacitor from the piezoelectric harvester at different pump conditions

The performance of this designed system is moreover investigated for condition monitoring application. It is worthy to note the microprocessor consumes 28.05 µW (8.5 µA and 3.3 V). By considering the capacitor constant, e.g. 150 µF, a voltage drop occurs in the capacitor during operation of the microprocessor. Hence, a voltage level switch is considered that enables the microprocessor after 4.0 V to ensure the continuous operation of the microcontroller. As advantage of this level switch, Torah et al. [26] noticed the cold start problem during experiments, where PIC microcontroller drew significant power as the voltage reached to a specific value. This level switch addresses the cold start problem. After the microprocessor starts operating, the microprocessor enables the RF transmitter for a period of time when the voltage reaches to a specific figure. During the transmission, the RF transmitter consumes 7 mA current. For this simulation, the PIC microcontroller enables the RF transmitter when the storage capacitor reaches to 7 V for a duration of 0.02 s. By considering the voltage equation across the capacitor with C= 150 µF, the voltage drop during the transmission time is calculated as 0.93 V. After the transmission period, the storage capacitor is charged by the piezoelectric harvester. Nevertheless, the charging time to reach 8 V depends on the voltage generation by the piezoelectric, which is different for different pump working conditions. The storage capacitor voltage during the full operation from the initial conditions are shown in Fig. 18. In this work, to include unknown errors during the operation, 2% random error is added to the capacitor voltage. As shown,

due to less pump acceleration during the defect-free condition, the charging process is slower than the other conditions; so that the first RF transmission occurred at 1.18 s. On the other hand, the water pump acceleration is higher for the defected conditions. Therefore, the first transmission time and the time intervals between the transmissions are significantly lower compared to the defect-free condition.

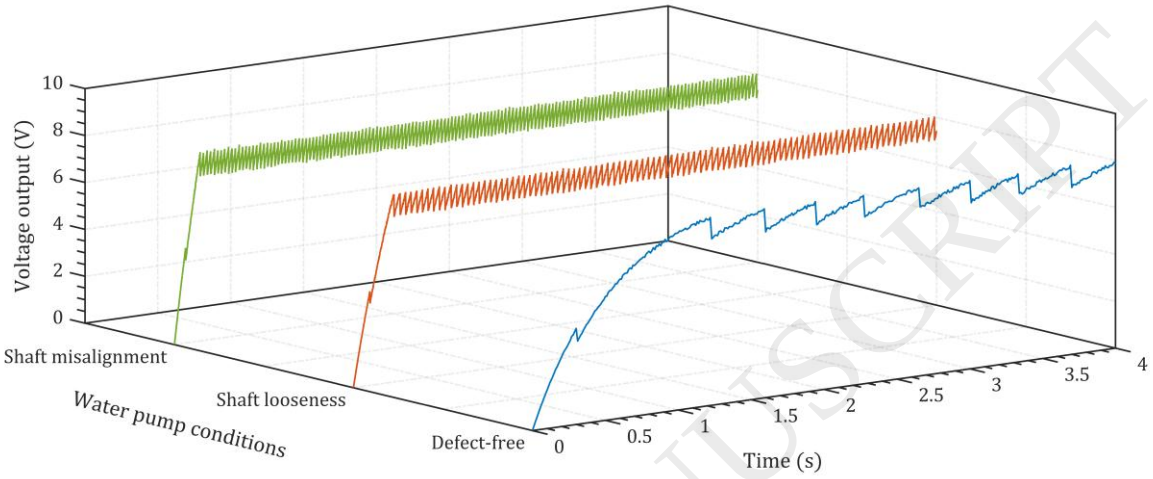

Fig. 18. Voltage output from storing capacitor during full operation for different water pump conditions

The elapsed times between the RF transmissions are shown in Fig. 19 for different water pump conditions. While the first transmission for the defect-free occurs at 1.18 s, it happens after 277 and 177 ms for shaft looseness and misalignment conditions, respectively. More important than the first transmission is the time between the transmissions as it is directly proportional to the charging process which is linked to the water pump acceleration. The elapsed time values between the transmissions are 350, 39 and 25 ms for the defect-free, shaft looseness and shaft misalignment conditions, respectively. Therefore, if the water pump condition changes from the defect-free to one of these faults, the elapsed time between the transmissions decreases immediately.

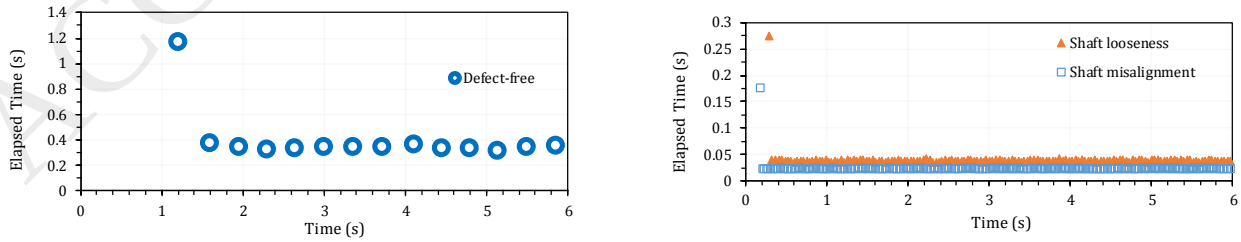

Fig. 19. The elapsed time between the RF transmissions for (a) defect-free and (b) defected conditions

To analysis the elapsed time data from Fig. 19, the parameters in Eq. (1) are obtained as $\mu = 0.350$, $\tau_0 = 0, \tau_1 = -0.311, \tau_2 = -0.326, \sigma_1 = 1.63E-2, \sigma_2 = 1.39E-3$ and $\sigma_3 = 9.98E-4$. Since a statistical model for the elapsed time for the different operating conditions was obtained, the state of water pump was conditioned by calculating the FI and $\mathcal{S}$ using Eq. (2) and (4).

In order to demonstrate possibility of the procedure, one case is considered in which the state of the water pump changes from the defect-free to the shaft misalignment in a duration of 20 s. Fig. 19 (a) shows the reconstructed time signals. Here a 5% random noise is added to the data in order to test the performance of the system in case of noisy environment. For 2-second interval, the FFT is applied on the signals and the contribution of 1X=49.5 Hz in the signal is extracted. This mode contribution is within the range of 0.50 m/s^{-2} in the defect-free condition to 1.53 m/s^{-2} in the shaft misalignment condition. The 1X contribution is fed into the bimorph piezoelectric model, Eq. (18), with the calculated optimum load resistance of $(R_l)_{opt}$=44600 Ω. Range of the piezoelectric voltage output is from 1.9 V in the defect-free to 5.8 V in the shaft-misalignment conditions. Moreover, the voltage generation from the bimorph is considered as the input for the optimum MDCP circuit and the voltage outputs are obtained using simulation. The final voltage in the storage capacitor ranges from 9.0 V to 28.3 V for the defect-free and shaft misalignment conditions, respectively. Fig. 19 (b) shows the 1X mode contribution, piezoelectric voltage and MDVM voltage output over ten 2-second period intervals. According to the immediate capacitor voltage, the elapsed time between the transmissions are calculated upon which the FI, CL and machine state $\mathcal{S}$ are obtained through Eq. (2) to (4), respectively. Fig. 19 (c) shows the FI of the water pump and the CL for this index over 20 s period. As shown for a duration of 8 s, from 1st to 4th 2-second intervals, the FI lies closely on 0 value. However, once the machine condition changes to the transition operation and the acceleration increases, the FI tends to rise from 0. The FI further increases until reaches to a symptom value for the shaft misalignment condition. The CL, which is an accuracy indicator for the condition monitoring process, is always close to 1 except for transition period which is dramatically less than the other values. Consequently, the machine state $\mathcal{S}$ is shown in Fig. 19 (d) with elapsed time over this 20 s time period. It can be seen that, the state of the water pump is correctly identified as "3" state through the faulty operation, which corresponds to the shaft misalignment. However, during the transition period, the system identified "2" for the machine state which is not correct. By considering the CL values for transition period, one can avoid from incorrect conditions of the machine.

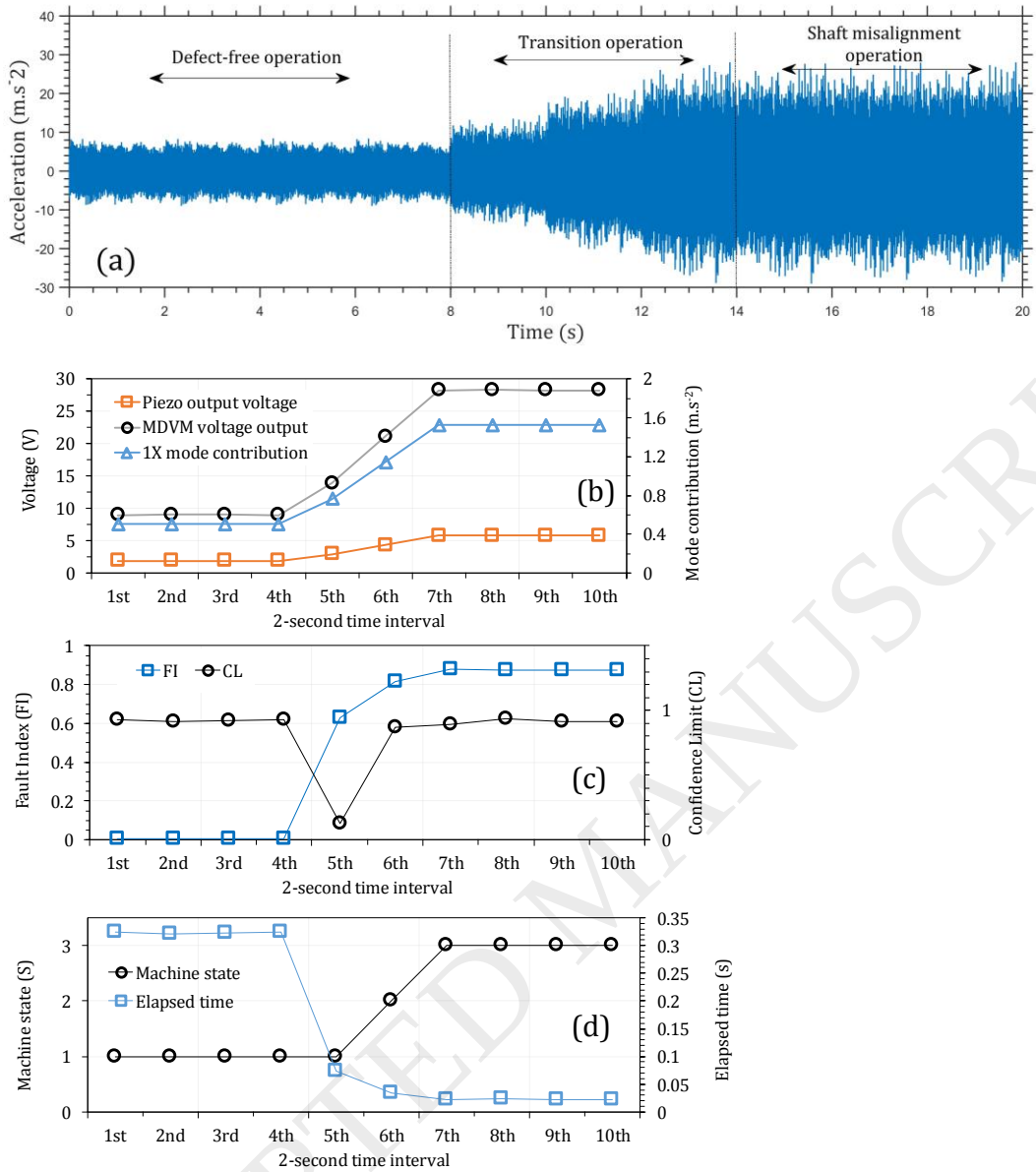

Fig. 20. The process of condition monitoring for a simulated case from reconstructed signals of the water pump. (a) Time signals, (b) 1X mode contribution from FFT and voltage output from harvesting unit, (c) FI and CL and (d) Water pump state and elapsed times between transmissions

6. Conclusions

In this study, a self-powered condition monitoring system is designed to perform operational condition monitoring based on the RF transmission pulses. After design of the system, an energy harvesting unit is proposed to provide sufficient energy and voltage level for this system. This energy harvesting unit comprises a piezoelectric bimorph harvester and Voltage Multiplier circuit. For this

study, input acceleration, which is a signal consisting of harmonics from a frequency range, is decomposed into a series of harmonic function using FFT. A distributed parameter model of piezoelectric harvester was used to estimate the output voltage. For the machine condition monitoring, a pulse-based approach has been proposed relying on the analysis of elapsed times between the RF transmission pulses. The performance of this system has been demonstrated for condition monitoring of a water pump. The designed system has been applied on experimental vibration signals captured from the water pump and shown that the water pump condition can be monitored during the operation. This system can be applied on larger network of machines for autonomous condition monitoring.

References

[1] S. W. Doebling, C. R. Farrar, and M. B. Prime, "A Summary Review of Vibration-Based Damage Identification Methods," *Shock Vib. Dig.*, vol. 30, no. 2, pp. 91–105, 1998.

[2] O. Janssens *et al.*, "Convolutional Neural Network Based Fault Detection for Rotating Machinery," *J. Sound Vib.*, vol. 377, pp. 331–345, 2016.

[3] C. Ruiz-Cárcel, V. H. Jaramillo, D. Mba, J. R. Ottewill, and Y. Cao, "Combination of process and vibration data for improved condition monitoring of industrial systems working under variable operating conditions," *Mech. Syst. Signal Process.*, vol. 66–67, pp. 699–714, 2016.

[4] A. Ragab, S. Yacout, M. S. Ouali, and H. Osman, "Prognostics of multiple failure modes in rotating machinery using a pattern-based classifier and cumulative incidence functions," *J. Intell. Manuf.*, vol. 30, no. 1, pp. 255–274, 2019.

[5] A. Moosavian, M. Khazaee, H. Ahmadi, M. Khazaee, and G. Najafi, "Fault diagnosis and classification of water pump using adaptive neuro-fuzzy inference system based on vibration signals," *Struct. Heal. Monit.*, vol. 14, no. 5, pp. 402–410, 2015.

[6] Y. T. Im, S. G. Doo, and J. S. Hwang, "Condition monitoring of cooling tower fan using K-band Doppler radar," *Microw. Opt. Technol. Lett.*, vol. 61, no. 1, pp. 158–162, 2019.

[7] A. Simm, Q. Wang, S. Huang, and W. Zhao, "Laser based measurement for the monitoring of shaft misalignment," *Meas. J. Int. Meas. Confed.*, vol. 87, pp. 104–116, 2016.

[8] J. Zhong *et al.*, "Vision-based system for simultaneous monitoring of shaft rotational speed and axial vibration using non-projection composite rfinge pattern," *Mech. Syst. Signal Process.*, vol. 120, pp. 765–76, 2019.

[9] J. Huang, G. Chen, L. Shu, H. Lin, and K. Liu, "Designing wireless vibration monitoring system for petrochemical units fault diagnosis," *Proc. - 2015 IEEE 12th Int. Conf. Ubiquitous Intell. Comput. 2015 IEEE 12th Int. Conf. Adv. Trust. Comput. 2015 IEEE 15th Int. Conf. Scalable Comput. Commun. 20*, pp. 582–588, 2016.

[10] J. Neuzil, O. Kreibich, and R. Smid, "A distributed fault detection system based on IWSN for machine condition monitoring," *IEEE Trans. Ind. Informatics*, vol. 10, no. 2, pp. 1118–1123, 2014.

[11] S. Cao and J. Li, "A survey on ambient energy sources and harvesting methods for structural health monitoring applications," *Adv. Mech. Eng.*, vol. 9, no. 4, p. 168781401769621, 2017.

[12] C. De Marqui and A. Erturk, "Electroaeroelastic analysis of airfoil-based wind energy harvesting using piezoelectric transduction and electromagnetic induction," *J. Intell. Mater. Syst. Struct.*, vol. 24, no. 7, pp. 846–854, 2013.

[13] H. Li, C. Tian, and Z. D. Deng, "Energy harvesting from low frequency applications using piezoelectric materials," *Appl. Phys. Rev.*, vol. 1, no. 4, pp. 0–20, 2014.

[14] M. Khazaee, A. Rezaniakolaei, and L. Rosendahl, "An experimental study on macro Piezoceramic fiber composites for energy harvesting," *Mater. Sci. Forum*, vol. 951, pp. 3–8, 2019.

[15] P. Cahill, B. Hazra, R. Karoumi, A. Mathewson, and V. Pakrashi, "Vibration energy harvesting based monitoring of an operational bridge undegoing forced vibration and train passage," *Mech. Syst. Signal Process.*, vol. 106, pp. 265–283, 2018.

[16] C. Maruccio, G. Quaranta, L. De Lorenzis, and G. Monti, "Energy harvesting from electrospun piezoelectric nanofibers for structural health monitoring of a cable-stayed bridge," *Smart Mater. Struct.*, vol. 25, no. 8, p. 085040, 2016.

[17] X. Zhao *et al.*, "Self-powered triboelectric nano vibration accelerometer based wireless sensor system for railway state health monitoring," *Nano Energy*, vol. 34, no. February, pp. 549–555, 2017.

[18] D. Lim, S. C. Mantell, and P. J. Seiler, "Wireless Structural Health Monitoring of Wind Turbine Blades Using an Energy Harvester as a Sensor," *32nd ASME Wind Energy Symp.*, vol. 000, no. 00, pp. 1–10, 2010.

[19] T. H. Owen, S. Kestermann, R. Torah, and S. P. Beeby, "Self powered wireless sensors for condition monitoring applications," *Sens. Rev.*, vol. 29, no. 1, pp. 38–43, 2009.

[20] D. Lim, S. C. Mantell, P. J. Seiler, and R. Yang, "Wind Turbine Blades as a Strain Energy Source for Energy Harvesting," in *51st AIAA Aerospace Sciences Meeting including the New Horizons Forum and Aerospace Exposition*, 2013, no. January, pp. 1–8.

[21] D.-W. Lim, S. C. Mantell, and P. J. Seiler, "Wireless monitoring algorithm for wind turbine blades using Piezo-electric energy harvesters," *Wind Energy*, vol. 20, no. 3, pp. 551–565, 2017.

[22] S. S. R. Patange, S. Raja, M. P. Vijayakumar, and V. R. Ranganath, "Study on low frequency energy harvesting system in laminated aluminum beam structures with delamination," *J. Mech. Sci. Technol.*, vol. 32, no. 5, pp. 1985–1993, 2018.

[23] W. W. Clark, J. R. Romeiko, D. a Charnegie, G. Kusic, and C. Mo, "A case study in energy harvesting for powering a wireless measurement system," *Struct. Heal. Monit. 2007 Quantif. Validation, Implementation, Vols 1 2*, no. September 2007, pp. 1765–1772, 2007.

[24] "https://www.microchip.com," *Date Accessed March 2019.* .

[25] O. O. Esu, S. D. Lloyd, J. A. Flint, and S. J. Watson, "Feasibility of a fully autonomous wireless monitoring system for a wind turbine blade," *Renew. Energy*, vol. 97, pp. 89–96, 2016.

[26] R. N. Torah, M. J. Tudor, K. Patel, I. N. Garcia, and S. P. Beeby, "Autonomous low power microsystem powered by vibration energy harvesting," *Proc. IEEE Sensors*, pp. 264–267, 2007.

[27] Https://www.rfsolutions.co.uk/, "RTFQ1P."

[28] H. A. Sodano, D. J. Inman, and G. Park, "Comparison of Piezoelectric Energy Harvesting Devices for Recharging Batteries," *J. Intell. Mater. Syst. Struct.*, vol. 16, no. 10, pp. 799–807, 2005.

[29] M. Kim, J. Dugundji, and B. L. Wardle, "Efficiency of piezoelectric mechanical vibration energy harvesting," *Smart Mater. Struct.*, vol. 24, no. 5, p. 055006, 2015.

[30] F. Pan and T. Samaddar, *Charge pump circuit design*. McGraw-Hill Professional, 2006.

[31] F. K. Shaikh and S. Zeadally, "Energy harvesting in wireless sensor networks: A comprehensive review," *Renew. Sustain. Energy Rev.*, vol. 55, pp. 1041–1054, 2016.

[32] T. V Galchev, J. McCullagh, R. L. Peterson, and K. Najafi, "Harvesting traffic-induced vibrations for structural health monitoring of bridges," *J. Micromechanics Microengineering*, vol. 21, no. 10, p. 104005, 2011.

[33] A. Erturk and D. J. Inman, "An experimentally validated bimorph cantilever model for piezoelectric energy harvesting from base excitations," *Smart Mater. Struct.*, vol. 18, no. 2, p. 025009, 2009.

[34] D. Young and R. P. Felgar, "Tables of characteristic functions representing normal modes of vibration of a beam," *University of Texas Engineering Research series*, vol. 44. pp. 1–31, 1949.

[35] J. W. Cooley, P. W. Lewis, and P. D. Welch, "The Fast Fourier Transform and its Applications," *IEEE Trans. Educ.*, vol. 12, no. 1, pp. 27–34, 1969.

[36] S. Roundy, P. K. Wright, and J. Rabaey, "A study of low level vibrations as a power source for wireless sensor nodes," *Comput. Commun.*, vol. 26, no. 11, pp. 1131–1144, 2003.

[37] N. E. DuToit and B. L. Wardle, "Experimental Verification of Models for Microfabricated Piezoelectric Vibration Energy Harvesters," *AIAA J.*, vol. 45, no. 5, pp. 1126–1137, 2007.

Majid Khazaee received his Bachelor and Master of Technology from Amirkabir University of Technology (Tehran Polytechnic) in 2013 and 2016. He is currently pursuing PhD in Energy Technology at Aalborg University, Aalborg, Denmark and is working on piezoelectric energy harvesters for autonomous sensors and actuators. He worked as senior project engineer in AS industrial group, during 2016-2017 on production line installation. His current research interests include low-power vibration harvesting piezoelectric harvester design, industrial vibration, autonomous condition monitoring and dynamical modeling of systems.

Alireza Rezaniakolaei was born in Babol, Iran, on August 04, 1983. He is an Associates Professor of energy technologies. He is head of Low Power Energy Harvesting & i-Solutions Research Programme at Department of Energy Technology, Aalborg University, Denmark with 10 years experiences in this field. His current research interests include fluid mechanics, thermal engineering and energy harvesting technologies, micro heat-transfer surfaces and integration of these technologies with renewable systems, actuators and sensor applications.

Ashkan Moosavian was born in 1988 in Tehran/Iran, received his B.Sc. and M.Sc. degrees in Agricultural Machinery Engineering from the Tehran University, Iran, in 2010 and 2012. He received PhD from Trbiat Modares University in Tehran/Iran. He is now senior test engineer in Irankhodro Powertrain Company (IPCO). His research fields include Application of Support Vector Machine and Neural Network in Mechanical Systems, Artificial Intelligence, Condition Monitoring, Fault Diagnosis, Application of Mechatronic in Agricultural Engineering.

Lasse A. Rosendahl was born in Ribe, Denmark, on October 13, 1967. He received the M.Sc.M.E. and Ph.D.M.E. Degrees from Aalborg University, Aalborg, Denmark. From 1998 to 1999, he was with the Department of Energy Technology (ET), Aalborg University, as an Assistant Professor, where he was an Associate Professor from 2000 to 2007, and has been a Professor since 2007. He is leader of Biomass Research Programme at ET. His current research interests include fluid mechanics, thermal energy technology, liquid biofuels and novel energy technologies, including modeling, simulation, and design with focus on optimized efficiency.